# Ultrasound Enhanced Diffusion in Hydrogels: An Experimental and Non-Equilibrium Molecular Dynamics Study

Sebastian E. N. Price,[1] Caroline Einen,[2] Othonas A. Moultos,[3] Thijs J. H. Vlugt,[3] Catharina de Lange Davies,[4] Erika Eiser,[2] and Anders Lervik[5]

[1)] *PoreLab and Department of Chemistry, The Norwegian University of Science and Technology NTNU, N7491 Trondheim, Norway.*

[2)] *PoreLab and Department of Physics, The Norwegian University of Science and Technology, NTNU, N7491 Trondheim, Norway.*

[3)] *Engineering Thermodynamics, Process & Energy Department, Faculty of Mechanical Engineering, Delft University of Technology, Leeghwaterstraat 39, 2628 CB Delft, The Netherlands*

[4)] *Department of Physics, The Norwegian University of Science and Technology, NTNU, N7491 Trondheim, Norway.*

[5)] *PoreLab and Department of Chemistry, The Norwegian University of Science and Technology, NTNU, N7491 Trondheim, Norway.*

(*Electronic mail: sebastian.n.price@ntnu.no)

Focused ultrasound has experimentally been found to enhance the diffusion of nanoparticles, our aim with this work is to study this effect closer using both experiments and non-equilibrium molecular dynamics. Measurements from single particle tracking of 40 nm polystyrene nanoparticles in an agarose hydrogel with and without focused ultrasound are presented and compared with a previous experimental study using 100 nm polystyrene nanoparticles. In both cases we observed an increase in the mean square displacement during focused ultrasound treatment. We developed a coarse-grained non-equilibrium molecular dynamics model with an implicit solvent to investigate the increase in the mean square displacement and its frequency and amplitude dependencies. This model consists of polymer fibers and two sizes of nanoparticles, and the effect of the focused ultrasound was modelled as an external oscillating force field. A comparison between the simulation and experimental results shows similar mean square displacement trends, suggesting that the particle velocity is a significant contributor to the observed ultrasound-enhanced mean square displacement. The resulting diffusion coefficients from the model are compared to the diffusion equation for a two-time continuous time random walk. The model is found to have the same frequency dependency. At lower particle velocity amplitude values, the model has a quadratic relation with the particle velocity amplitude as described by the two-time continuous time random walk derived diffusion equation, but at higher amplitudes, the model deviates, and its diffusion coefficient reaches the non-hindered diffusion coefficient. This observation suggests that at higher ultrasound intensities in hydrogels, the non-hindered diffusion coefficient can be used.

Author accepted manuscript version of article in
*The Journal of Chemical Physics 160 (2024). DOI: 10.1063/5.0202182* .



## I. INTRODUCTION

A major problem in cancer treatment based on chemotherapy, is the low and heterogeneous drug uptake in tumors. Encapsulating drugs into nanoparticles (NPs) increases their accumulation in the tumor due to its hyperpermeable capillaries, and reduces toxic effects in normal tissue[1]. However, the NPs are heterogeneously distributed and mainly located close to the vessel walls in the tissue. After crossing the capillary wall, the NPs have to penetrate through the extracellular matrix, which consists of a collagen fiber network embedded in a hydrophilic gel of glycosaminoglycans, constituting a major barrier for successful delivery[2,3]. Various strategies have been proposed to improve the delivery of drugs and NPs for cancer treatment[4]. One approach is the use of focused ultrasound (FUS), which has been shown to improve the delivery of drug-loaded NPs[5].

Several mechanisms have been proposed to explain the improved delivery[4]. One of these is ultrasound enhanced diffusion, which is a rise in the diffusion coefficient when applying FUS. We have recently observed this mechanism when experimentally studying the transport of 100 nm sized polystyrene NPs exposed to ultrasound in a hydrogel[6]. Several other research groups have also observed an ultrasound-enhanced increase in diffusion[7–11].

The research team at the University of Vermont proposed that the diffusion coefficient can be divided into two terms, a molecular diffusion coefficient and an oscillatory diffusion coefficient, which comes from the ultrasound forcing. In one of their earlier papers[9], a stochastic model proposed by Marshall [12] was used to describe the oscillatory diffusion coefficient. The stochastic model assumes that the enhanced diffusion can be explained by a combination of acoustic advection oscillations and random retention, caused by the steric hindrance from the pore walls in a porous media, such as the extracellular matrix of tumor tissue. In a more recent publication[11], the stochastic model proposed by Balakrishnan and Venkataraman [13] is used to explain the oscillatory diffusion coefficient. Balakrishnan and Venkataraman [13] considered the problem of a particle that randomly flips between two states of either oscillation or a constant random walk and used the continuous-time random walk (CTRW) theory to derive an

equation for the oscillatory diffusion coefficient. In both models, anomalous diffusion was not considered. We observed anomalous sub-diffusion from the mean square displacement (MSD) data in our previous work[6]. Here, we investigate the effect of FUS on both anomalous and normal diffusion in a poroelastic medium. To achieve this, we conduct a comparative analysis between our experimental findings and a non-equilibrium molecular dynamics (NEMD) simulation in order to better understand the underlying mechanism behind the enhanced diffusion.

To the best of our knowledge, there is only one study in which molecular dynamics was used to specifically investigate diffusion under ultrasound exposure. In this study, Yang, Zhang, and Qiao [14], investigated the diffusion of aluminum and copper atoms at the interface during ultrasonic welding. However, there appears to be no molecular dynamics study of the impact of ultrasound on diffusion for a medical application and in soft porous media. A better understanding of the underlying mechanisms of the enhanced diffusion is essential in order to optimize the FUS-increased particle transport. NEMD can advance this understanding by enabling the study of a highly controlled system, facilitating the measurement of the impact of individual mechanisms in isolation.

In this paper, we present experimental data for the MSD of NPs in an agarose gel exposed to FUS. We simulated the effect of FUS by adopting the method proposed by Zhang *et al.* [15], in which we apply an external oscillating force that acts unidirectionally on the particles. The choice of an oscillating force is based on the proposition by Marshall [12], suggesting that the enhanced diffusion is primarily due to the combination of oscillatory flow and hindrance. We have used a model similar to the one presented by Yu *et al.* [16] for the porous medium. Our model is reparameterized for an implicit solvent, which allows us to reach long time scales in our molecular dynamics simulations. We study two different NPs of different sizes (small and large) in our simulations. The small NP is used to study normal diffusion, while the large NP (created by joining 16 of the smaller particles in a globular shape) is used to study anomalous diffusion. We show that NEMD can reproduce the trends of experimental MSD results. We also show that the theoretical model derived by Balakrishnan and Venkataraman [13] agrees with the NEMD model for lower FUS amplitudes. These findings support the usage of this model for interpreting FUS experiments.

We begin our paper by presenting our experimental procedure in section II and introducing our simulation model and protocol in section III. This is followed by our results and discussion in section IV, where we compare our simulations to the experiments and theoretical model.

## II. EXPERIMENTAL

We performed single particle tracking (SPT) of 40 nm polystyrene NPs during FUS exposure in an agarose hydrogel with added evaporated milk and compared our results to our previous study of larger 100 nm particles in the same hydrogel[6]. Briefly, agarose powder (Agarose, BioReagent, for molecular biology, low EEO, Sigma-Aldrich, St. Louis, MO, USA) was dissolved in 1 mM phosphate buffered saline (PBS) (Phosphate buffered saline tablets, Sigma-Aldrich) at boiling temperature and cooled to 50 °C. Next, evaporated milk (Tørsleffs® condensed milk, unsweetened, Hvidovre, Denmark) and 40 nm large, red fluorescent polystyrene NPs from FluoSpheres® (580/605 emission range) with carboxylate surface-modification were added to a concentration of 2% ($w/v$) agarose, 10% ($v/v$) evaporated milk and 0.25 ţg mL$^{-1}$ NPs. The NPs were purchased from Thermo Fisher Scientific (Waltham, MA, USA). The solution was cast in disk shaped molds 9 mm in radius and 0.9 mm in height, and kept in 1 mM PBS with 0.25 ţg mL$^{-1}$ NPs at 4 °C until use within 24 h.

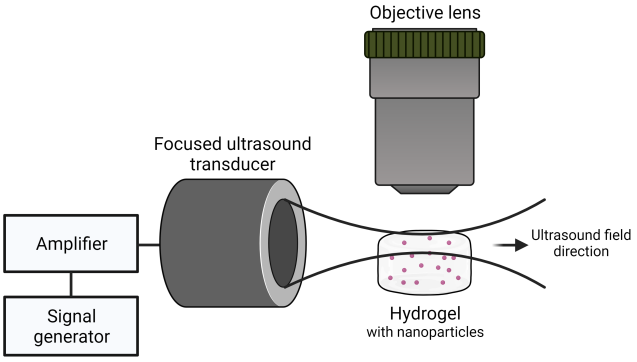


FIG. 1: Simplified illustration of the experimental setup for confocal imaging of fluorescent NPs in a hydrogel sample during FUS exposure. Focused ultrasound is sent by a transducer through the hydrogel with NPs in a buffer filled sample holder (not shown). Movement of NPs in the hydrogel is captured using a confocal microscope before and during ultrasound exposure. Created with BioRender.com.

We imaged NPs using a confocal microscope (LSM 700, Zeiss, Oberkochen, Germany) with a 40X dip-in objective (W Plan Apochromat 40X/1.0 DIC M 27, Zeiss) in a 40 ţm × 40 ţm imaging frame. The NP fluorophore was excited by a 555 nm laser, with detection above 559 nm. The agarose hydrogel sample was placed in a custom sample holder filled with 1 mM PBS for NP imaging during FUS exposure in an imaging plane parallel to the ultrasound propagation direction, sketched in Figure 1. Due to the confinement by the hydrogel, the NPs moved slowly compared to the expected motion in a free buffer solution. The frame rate, was therefore, limited to 17.9 fps to capture NP movement in the hydrogel. The NPs were imaged for 5 min before and during FUS exposure with a 1 MHz focused transducer (center frequency 1 MHz, focal depth 73.5 mm, diameter 60 mm, Precision Acoustics, Dorchester, UK) excited by a signal generator (33500 B, Keysight Technologies, Santa Rosa, CA, USA) through an amplifier (50 dB 2100L, E&I Ltd., Rochester, NY, USA). The hydrogel was exposed to pulsed FUS of 20% duty cycle (DC) with a pulse repetition frequency of 1 Hz. The FUS induced a slight shift of focus in the sample, such that the particles were moved out of the field of view while the ultrasound was on. The DC was, therefore, limited to 20% to ensure sufficient track-

ing of the particles between imaging frames. A peak negative pressure of 1 MPa ($I_{SPTA} = 6.76\,W/cm^2$) was applied, and the pressure was assumed to be uniform within the imaging field. The motion of NPs was followed using Trackpy[17], where the minimum tracking time was set to 0.5 s to filter out noise and spurious particles. Three hydrogel samples were used to capture videos before and during FUS exposure, and the resulting particle tracks were combined to calculate the ensemble MSD of NPs without and during FUS exposure, respectively.

## III. NEMD SIMULATIONS

### A. Hydrogel System

Agarose hydrogels consist of cross-linked, semiflexible fibers that are formed from self-assembled polysaccharide chains. The thickness ranges from 20 to 30 nm, and the lengths can reach several hundred nanometers, depending on the concentration[18]. The NPs that were used in our experiments ranged from 40 to 100 nm and a full-atomistic simulation would thus be prohibitively computationally expensive. We, therefore, use a coarse-grained NEMD simulation using the LAMMPS software[19]. Our model, analogous to the work established by Yu *et al.* [16], comprised 10 NPs and 25 cross-linked polymer fibers. Each polymer fiber was composed of 100 beads, each with an individual mass $m = 8.5$ MDa and a diameter $\sigma = 30$ nm. The interconnections between these beads were described by harmonic bond and angle potentials. The respective spring and bending constants were set to $k_b = 100\varepsilon/\sigma^2$ and $k_\theta = 100\varepsilon$, respectively; $\varepsilon$ represents an energy parameter with value $\varepsilon/k_B = 267$ K, where $k_B$ is the Boltzmann constant. The bond length was set to $r_0 = \sigma$, and the equilibrium bond angle was set to $\theta_0 = 2\pi/3$ so that a relatively coiled up structure mimicking the real network would be obtained. We introduced two distinct NP sizes into our simulation setup. The smaller NP consisted of one particle with a mass of $1m$, while the larger NP was constructed by positioning 16 rigid particles on a face-centered cubic (FCC) lattice. The arrangement yielded a globular NP density of $0.9/\sigma^3$.

TABLE I: Parameters (in LJ-units) used for the NEMD equilibration step of the system with dimensions $30.5\sigma \times 30.5\sigma \times 30.5\sigma$ consisting of 10 NPs, 25 polymer fibers and 22 500 solvent particles.

| Particle 1 | Particle 2 | Potential | Epsilon | Sigma |
|---|---|---|---|---|
| NP | NP | WCA | $0.5\varepsilon$ | $1\sigma$ |
| | Polymer | WCA | $0.5\varepsilon$ | $1\sigma$ |
| | Solvent | LJ | $1.5\varepsilon$ | $1\sigma$ |
| Polymer | Polymer | WCA | $1.0\varepsilon$ | $1\sigma$ |
| | Solvent | LJ | $2.0\varepsilon$ | $1\sigma$ |
| Solvent | Solvent | LJ | $2.0\varepsilon$ | $1\sigma$ |

The system was initiated by randomly placing both the polymer chains and NPs into a simulation box and immersing them in a solvent made of 22,500 solvent particles, each one with a mass of $1m$. All particle interactions were modelled using either the Lennard-Jones (LJ) potential or the Weeks-Chandler-Andersen (WCA) soft sphere potential[23]. The parameters used for equilibration are listed in Table I. To achieve system equilibrium, we used a Nosé-Hoover barostat[23] to reach a reduced pressure of $P^* = P\sigma^3/\varepsilon = 0$ and a Nosé-Hoover thermostat[23] to attain a reduced temperature of $T^* = Tk_B/\varepsilon = 1.1$. These are the same state-variable values as the ones used by Yu *et al.* [16]. Periodic boundary conditions were applied in all spatial directions. Throughout all simulations, a consistent time step, $d\tau = 0.007\tau$, where $\tau = \sigma(m/\varepsilon)^{1/2}$, was used. During the equilibration phase, we allowed 10 %

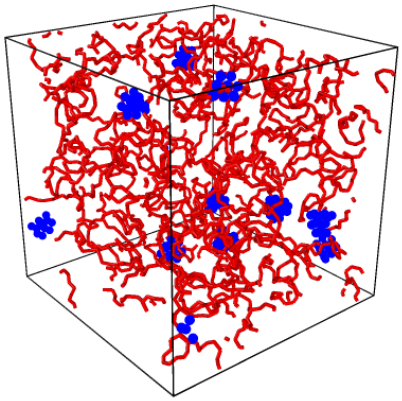

FIG. 2: A snapshot from the simulation of the system with dimensions $30.5\sigma \times 30.5\sigma \times 30.5\sigma$ showing large NPs (blue) diffusing in the gel network (red). The system was visualized using the OVITO software[20].

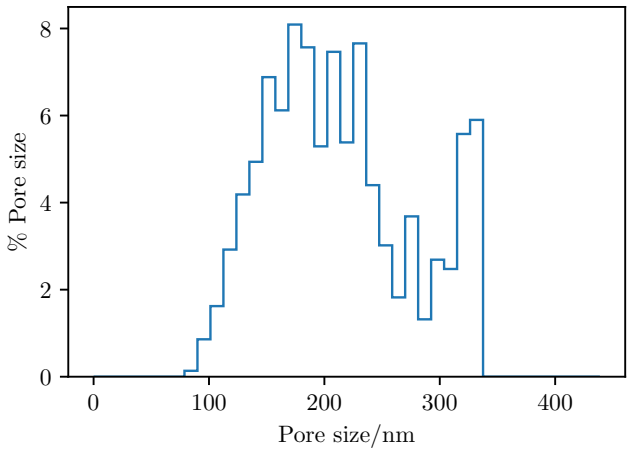


FIG. 3: Pore size distribution averaged over five different initialized gel networks, calculated using a Monte Carlo approach that employed the Voronoi decomposition to map and characterize accessible void spaces. The analysis was performed using the Zeo++ code[21,22].

of the polymer beads to cross-link when two beads from different polymer chains came within a distance of $1.5\sigma$, same as Yu *et al.* [16]. After equilibration, the solvent particles were removed and the polymer fiber particles were individually tethered to their initial positions using a spring constant of $k_{\text{self}} = 20\varepsilon/\sigma^2$. An example of an equilibrated gel system is shown in Figure 2. To characterize the equilibrated gel system, we computed the pore size distribution through a Monte Carlo approach that employed the Voronoi decomposition to map and characterize the accessible void space. The analysis was conducted using the Zeo++ code[21,22]. Figure 3 displays the pore size distribution averaged over five different initialized gel systems. The distribution is Gaussian-like with a mean pore size of ca. 200 nm, consistent with previously reported experimental pore size distributions for agarose gels[24]. There is, however, a second peak at ca. 350 nm suggesting some heterogeneity in the structure, due to one larger pore.

Subsequent simulations were carried out in the canonical $NVT$-ensemble with an implicit solvent using a Langevin thermostat[23]. The Langevin damping parameter $k_{\text{damp}}$ was set to $3\text{d}\tau$, as a relatively low value was needed to keep the temperature stable during the NEMD simulations.

Following the initialization of the system, we made adjustments to the interaction parameters governing the interactions between the polymer fibers and the NPs. For the larger NPs, we set the LJ cutoff value to $r_c = 2.5\sigma$ and adjusted the well depth value to $0.9\varepsilon$. This value was chosen so that the large NPs would be sub-diffusive, but still able to occasionally move freely during the simulation. Similarly, for the smaller NPs, we set the cutoff value to $r_c = 2.5\sigma$, while adjusting the well depth value to $1.5\varepsilon$. This choice was made to deliberately generate a discernible difference in the MSD plot between the non-hindered and hindered gel systems, while at the same time avoiding that the small NPs become sub-diffusive. A summary of all the interaction parameters utilized to obtain the MSD data is presented in table II.

TABLE II: Parameters (in LJ-units) used to obtain the MSD data of the system with dimensions $30.5\sigma \times 30.5\sigma \times 30.5\sigma$ consisting of 10 NPs and 25 polymer fibers.

| Particle 1 | Particle 2 | Potential | Epsilon | Sigma |
|---|---|---|---|---|
| Large NP | Large NP | WCA | $0.5\varepsilon$ | $1\sigma$ |
| | Polymer | LJ | $0.9\varepsilon$ | $1\sigma$ |
| Small NP | Small NP | WCA | $0.5\varepsilon$ | $1\sigma$ |
| | Polymer | LJ | $1.5\varepsilon$ | $1\sigma$ |
| Polymer | Polymer | WCA | $1.0\varepsilon$ | $1\sigma$ |

### B. Ultrasound implementation

Several groups have attempted to simulate the effect of ultrasound using molecular dynamics[15,25–33]. Okumura and Itoh [25] studied how ultrasonic cavitation disrupts the amyloid fibrils of Alzheimers amyloid-$\beta$ peptides using NEMD by applying a sinusoidal Andersen barostat. Man *et al.* used a similar method in their work using a sinusoidal Berendsen barostat[26–28]. Alternative methods, not reliant on sinusoidal barostats, have also been proposed. FUS creates focused sinusoidal sound waves that pass through a medium of interest. The particles in the medium will have a particle velocity, which is the physical speed of a parcel of the medium as it moves back and forth in the direction the sound wave is traveling[34]. Zhang *et al.* [15] applied this sinusoidal particle velocity to the system to investigate the mechanism of heavy oil viscosity reduction by ultrasound. Marshall [12] proposed that the sinusoidal particle velocity combined with hindrance is the main contributor to the enhanced diffusion of NPs. Therefore, we opted for a method similar to Zhang *et al.* [15], where we added an external oscillating force field. The force field $F$ works on the particles in the $x$-direction and results in the particle velocity $v$,

$$v = 2\pi f A \cos(2\pi f t), \tag{1}$$

where $A$ is the amplitude of the velocity oscillation. $A$ is proportional to the ultrasound pressure, and $f$ is the ultrasound frequency. A video of the NEMD simulation during FUS exposure can be found in Figure 8 of the supplementary material (Multimedia view). The NEMD system has a length scale in the order of 100 nm, which is small relative to the ultrasound wavelength. The latter has a length scale in the order of 1 mm given as $c/f$, where $c$ is the speed of sound. We, therefore, assume that we can safely neglect the spatial variation of the ultrasound field.

## IV. RESULTS AND DISCUSSION

Here, we present the results from the experiments and the NEMD simulations. We first compare the simulation results with both the new 40 nm polystyrene NP MSDs and those for 100 nm, previously published[6] with and without FUS. Subsequently, we compare the results from the simulations with the two-time CTRW theory by Balakrishnan and Venkataraman [13]. Finally, we summarize our observations and comment on its implications for future work.

### A. Comparison of MSD between NEMD model and experiments

To obtain the MSDs, we performed simulations with the small NPs for 200 million time steps and the large NPs for 2 billion time steps. The MSDs were calculated using the Einstein relation combined with the order-$n$ algorithm for sampling via the LAMMPS plugin on-the-fly calculation of transport properties (OCTP)[35]. We performed simulations with and without FUS, where we tested various particle velocity values. As explained in section II, a DC of 20% was used during the FUS experiments, while the NEMD simulations had effectively a 100 % DC. To compare the NEMD simulations with the laboratory experiments, we made the following assumption: We postulated that during the 80 % of the time when the FUS is turned off, the NP MSD is equivalent to that

of the NPs in the absence of FUS ($MSD^{Gel}$). Conversely, during the remaining 20 % of the time, we assumed that the NPs have an ultrasound enhanced MSD ($MSD^{US}$). This can be formulated as follows:

$$MSD^{AV} = DC \times MSD^{US} + (1 - DC) \times MSD^{Gel}. \quad (2)$$

Here, $MSD^{AV}$ is the experimentally measured MSD during FUS exposure with a 20 % DC. This assumption is reasonable at a low pulse repetition frequency and a high DC, as the time it takes for the system to adjust between FUS being on or off will be small compared to the time it stays in that state. By rearranging Equation (2), we calculated the experimental $MSD^{US}$ by re-weighting the measured MSD data in the following way

$$MSD^{US} = \frac{MSD^{AV} - (1 - DC) \times MSD^{Gel}}{DC}. \quad (3)$$

The MSD results obtained from our single-particle tracking experiments are shown in Figure 4. In contrast to the 100 nm polystyrene NPs MSD, the MSD for 40 nm has a slope in the log-log plot closer to one indicating a less anomalous sub-diffusive behavior. Figure 4 shows that the application of FUS increases the MSD of the particles in both cases. In the short time scale regime, there is a larger difference between the MSD with and without FUS compared to the longer time scale, especially for the 100 nm particles. This could be due to an increase in the static positional error in particle tracking caused by FUS-induced vibrations in the experimental setup, resulting in a positive shift of the MSD at short time scales[36]. At longer time scales, the MSD of the 40 nm particles exposed to FUS exhibits a steeper slope on the log-log scale, compared to the case without FUS.

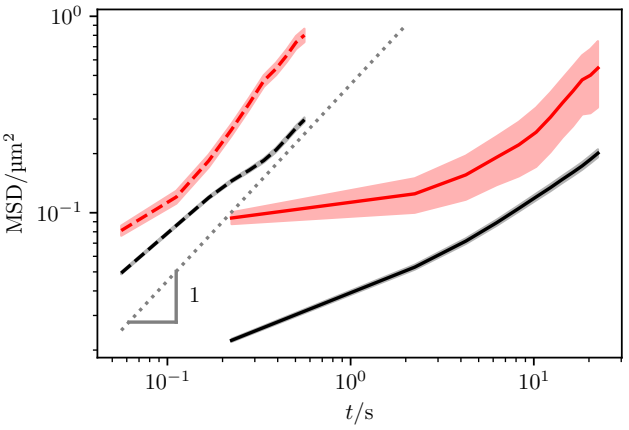


FIG. 4: Experimentally measured MSD as a function of time for 100 nm polystyrene NPs[6] indicated as the solid lines and for 40 nm polystyrene NPs indicated as the dashed lines. The black color is without FUS and the red color is with FUS. The shaded areas shows the standard error in the measurements. The gray dotted line is shown to illustrate a slope of one in the log-log scale.

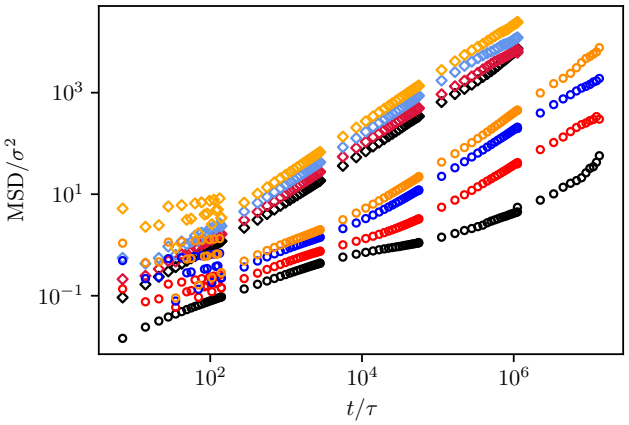


FIG. 5: MSD of NPs in a gel as a function of time from the NEMD simulations. The circles indicate the large NPs without FUS (black circles) and with FUS: $A = 0.15\sigma$ (red circles), $A = 0.30\sigma$ (blue circles) and $A = 0.45\sigma$ (orange circles). The diamonds indicate the small NPs without FUS (black diamonds) and with FUS: $A = 0.5\sigma$ (red diamonds), $A = 1.0\sigma$ (blue diamonds), and $A = 3.9\sigma$ (orange diamonds).

Figure 5 shows the MSD of the particles derived from our NEMD simulations. Consistent with the experimental findings in Figure 4, the large NPs in the NEMD simulations exhibit anomalous sub-diffusion, while the small NPs display normal diffusion within the error. This suggests that the NEMD simulation effectively captures some of the diffusive behavior of the NPs.

Upon applying a particle velocity, the MSD values show an increase for both NP sizes, as depicted by the colors red, blue, and orange in Figure 5. This is observed for particle velocity amplitudes $A = 0.15\sigma$, $A = 0.30\sigma$ and $A = 0.45\sigma$ for the large NPs and $A = 0.5\sigma$, $A = 1.0\sigma$ and $A = 3.9\sigma$ for the small ones. Notably, the large NPs exhibit an anomalous sub-diffusive behavior, although the effect is less pronounced when $A = 0.30\sigma$ and $A = 0.45\sigma$.

At time scales ca. in the order of $1/f$, which for Figure 5 will be in the order of 100 $\tau$, the MSD values for the NEMD simulation with a particle velocity display oscillations. This is a known phenomenon[37,38] which arises from the MSD sampling consistently occurring at the same displacement during time scales around the order of $1/f$, while over extended durations, these displacements become effectively smoothed or averaged. However, even at these extended time scales, a discernible rise in the MSD values persists and can be attributed to the displacement force pushing the NPs away from the gel fibers, facilitating freer movement. This effect intensifies with increasing amplitude. However, the NEMD simulations for the small NPs do not capture the steeper slope on the log-log scale as seen for the 40 nm FUS exposed particles in Figure 4. This is due to our NEMD model for the small NPs being already approximately Brownian, while the experimental 40 nm particles are slightly subdiffusive. This means that exposure to FUS in the NEMD simulations of the small NPs has an inappreciable effect on the slope.

In summary, our coarse-grained NEMD model qualitatively captures the MSD behavior observed experimentally. The introduction of a particle velocity to the particles increases the MSD values and reduces the anomalous sub-diffusive behavior, especially at higher particle velocity amplitudes. These findings suggest that the particle velocity itself plays a significant role as the primary contributor to the observed ultrasound enhanced diffusion coefficient. In future studies, it would be interesting to see if a more realistically parameterized model can accurately predict the experimental results.

### B. Comparison of diffusion coefficients from NEMD and two-time CTRW theory

The two-time CTRW theory does not apply to anomalous diffusion. We therefore used the case of small NPs for our comparison, as they do not display anomalous sub-diffusion as shown in Figure 5. The simulation time was set to 200 million time steps. The two-time CTRW theory, developed by Balakrishnan and Venkataraman [13], assumes that the particles randomly flip between two states, one of oscillatory motion and the other of constant random walk. From this assumption the following equation for the diffusion coefficient $D$ was derived:

$$D = D_0 + \frac{\langle x_A^2 \rangle}{2\tau_0} \left[ \frac{4\pi^2 \tau_0^2 f^2}{1 + 4\pi^2 \tau_0^2 f^2} \right]. \quad (4)$$

where $D_0$ is the diffusion coefficient when not in the oscillating state, $\tau_0$ is the average particle holding time in the oscillating state and $\langle x_A^2 \rangle$ is the mean square displacement of the particle in the oscillating state.

The diffusion coefficient was calculated for various particle velocity amplitudes by performing a linear regression at time scales where the MSD becomes a linear function. The diffusion coefficients as a function of particle velocity amplitudes are shown in Figure 6. The black circles indicate the diffusion coefficients from the NEMD simulations, the red line indicates the diffusion coefficient in a buffer solution from the NEMD simulations, and the black dashed line is the fitted quadratic function,

$$D = D_0 + cA^2, \quad (5)$$

where $c$ is a fitted coefficient with a dimension of inverse time. This is a simplification of equation (4) given by Balakrishnan and Venkataraman [13], where Karki, Marshall, and Wu [11] noted that $\langle x_A^2 \rangle^{1/2}$ will be proportional to the ultrasound amplitude, which we control through the particle velocity amplitude $A$. The coefficient $c$ was fitted to the NEMD diffusion coefficients, ranging from zero particle velocity amplitude to the final diffusion coefficient that yielded the smallest variance in the coefficient. Figure 6 shows that for lower values of $A$, the diffusion coefficient has a quadratic relationship with $A$. Karki, Marshall, and Wu [11] also obtained a similar agreement with Equation 5 from their experiments. However, for approximately $A = 1.0\sigma$, the trend deviates from a quadratic function, and the diffusion coefficient approaches the diffusion coefficient of the system without polymer fibers for larger amplitudes.

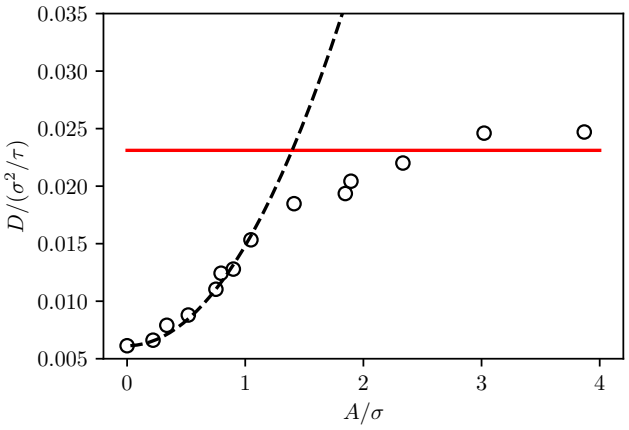


FIG. 6: Diffusion coefficients for small NPs in a gel as a function of the particle velocity amplitude. The black circles indicate the results from NEMD in a gel for different particle velocity amplitudes. The red horizontal line indicates the molecular dynamics diffusion coefficient in a non-hindered system. The black dashed line is a fitted model based on the equation from Balakrishnan and Venkataraman [13]. A frequency of 1 MHz was used for all the simulations. Each simulation was repeated three times (with different initial velocities), and the uncertainties were estimated from these three simulations. The uncertainties (error bars) are not visible, since they are smaller than the data point symbols.

One possible explanation for this deviation is that at higher particle velocity amplitudes, the attractive forces between the NPs and the polymer fibers become negligible compared to the acoustic force required to obtain the given particle velocity. At high particle velocity values, the acoustic force in our NEMD model is one order of magnitude greater than the attractive force between the polymer fibers and the NPs. Consequently, the polymer fibers do not represent any hindrance and increasing the particle velocity does not increase the diffusion. Instead the NPs enters the regime of ordinary non-hindered diffusion. The hindrance, as pointed out by Curran and Marshall [39] in their comparison between their stochastic model for oscillatory diffusion and the two-time CTRW theory, is essential for the oscillatory motion to increase the diffusion. It should also be mentioned that there was a slight increase in the reduced temperature with the increasing amplitude of the particle velocity. At the largest amplitude value of $3.9\sigma$, the reduced temperature increased from $1.1T^*$ to $1.26T^*$. This observation indicates that at higher $A$ values, the thermostat is unable to maintain a constant reduced temperature value of $1.1T^*$. In Figure 7, the diffusion coefficients, plotted as a function of frequency, were calculated for the small NPs using a particle velocity amplitude of $A = 0.9\sigma$. The black circles indicate the diffusion coefficients from the NEMD simu-

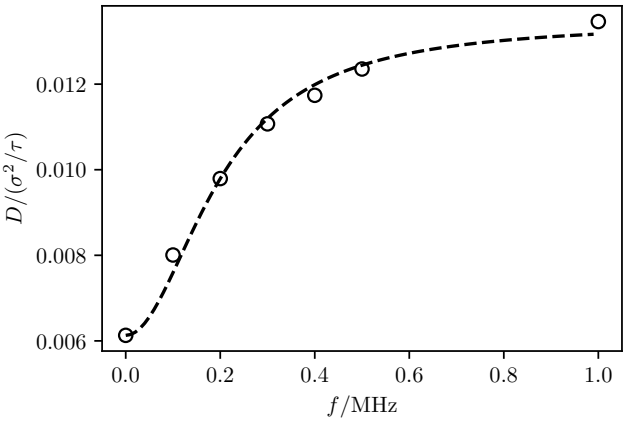


FIG. 7: Diffusion coefficients for small NPs in a gel as a function of US frequency. The black circles indicate the results from NEMD in a gel for different US frequencies. The black dashed line is a fitted model based on the equation from Balakrishnan and Venkataraman [13]. Each simulation was repeated three times (with different initial velocities), and the uncertainties were estimated from these three simulations. The uncertainties (error bars) are not visible, since they are smaller than the data point symbols.

lations, and the black dashed line is the fitted function,

$$D = D_0 + \frac{c_1 f^2}{1 + c_2 f^2}. \tag{6}$$

Here, $c_1$ and $c_2$ are fitted coefficients. This equation has the same frequency dependency as Equation (4), where $A$ is assumed constant. In this case, the NEMD simulations agree well with the two-time CTRW theory. The same was the case with the experimental work by Karki, Marshall, and Wu [11]. At the particle velocity amplitude $A = 0.9\sigma$, the two-time CTRW theory is expected to hold as shown in Figure 6, because at this point, the calculated diffusion coefficient is still a quadratic function of the particle velocity amplitude. Thus, the acoustic diffusion coefficient is in accordance with the two-time CTRW theory for both the amplitude up to approximately $1\sigma$ and frequency. Increasing the frequency above 0.6 MHz has a limited effect on the ultrasound-enhanced diffusion, and the diffusion coefficient for non-hindered small NPs is not reached. The maximal ultrasound-enhanced diffusion coefficient is determined by the $c_1/c_2$ ratio, as seen from Equation (6).

To summarize, the calculated diffusion coefficient from the coarse-grained model has the same oscillation frequency dependency as the two-time CTRW theory derived diffusion coefficient. For lower particle velocity amplitudes, the diffusion coefficient from the coarse-grained model has the same quadratic particle velocity amplitude dependency as the two-time CTRW theory derived diffusion coefficient, but reaches the diffusion coefficient of the non-hindered case at higher amplitude values. This is due to the hindrance becoming negligible in comparison with the oscillation force at higher amplitudes. These observations are interesting when optimizing ultrasound transducer settings for increased particle transport in viscoelastic materials, as it suggests that at sufficient high ultrasound intensities, the non-hindered diffusion coefficient can be used. At higher amplitude values, other effects that are not included in our model may become more dominant, such as the increase in temperature, potential structural changes in the gel network and ultrasound induced cavitation[40]. Future studies on high intensity ultrasound induced diffusion should incorporate these effects.

## V. CONCLUSION

We have performed single particle tracking of 40 nm polystyrene nanoparticles (NPs) in an agarose hydrogel with and without focused ultrasound (FUS) and compared it to our previous experimental study using 100 nm polystyrene NPs[6]. In both cases, we observed an increase in the mean squared displacement (MSD) during FUS. We have also created a coarse-grained implicit solvent non-equilibrium molecular dynamics (NEMD) model. This model consisted of polymer fibers and two sizes of NPs, with the effect of the FUS modelled as an external oscillating force field. Using this model, we performed simulations for different particle velocity amplitude values on both the small and large NPs. The MSD from these simulations was compared to the experimental MSD, and matching trends were observed. This suggests that the particle velocity is a significant contributor to the observed ultrasound-enhanced diffusion coefficient. The computed diffusion coefficients from the presented coarse-grained NEMD model were compared to the two-time continuous-time random walk (CTRW) theory derived diffusion equation by Balakrishnan and Venkataraman [13] and were found to have the same oscillation frequency dependency. For the lower amplitude values, the simulated diffusion coefficients also had a quadratic relation with the particle velocity amplitude, as described by the two-time CTRW theory. At higher amplitude values, the simulated diffusion coefficients diverged from the quadratic trend, and they approached the non-hindered diffusion coefficient value due to the hindrance interaction with the polymer fibers becoming negligible compared to the oscillation force. We hope that our observations on the ultrasound-enhanced diffusion can be used to optimize FUS enhanced drug transport and that, in the future, a similar NEMD model with more realistic parameters will be able to predict experimental ultrasound-enhanced diffusion coefficients.

## VI. SUPPLEMENTARY MATERIAL

See the supplementary material for a video file showing an example of a simulation of small NPs (blue) in a gel (red) system under FUS exposure with a particle velocity amplitude of $0.9\sigma$ is included here.

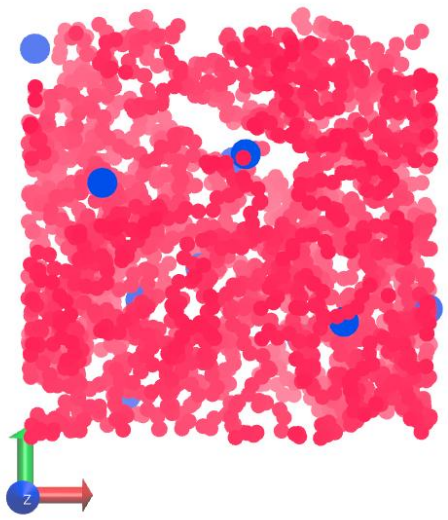


FIG. 8: (Multimedia view). An example of a simulation of small NPs (blue) in a gel (red) system under FUS exposure with a particle velocity amplitude of $0.9\sigma$. Visualized using VMD[41].

## ACKNOWLEDGMENTS

The authors would like to thank Magnus Gjennestad and Rune Hansen at SINTEF and Signe Kjelstrup at the Norwegian University of Science and Technology for fruitful discussions. This work was supported by the Research Council of Norway through project number 301581 and through its Centre of Excellence funding scheme, project number 262644, PoreLab.

## VII. AUTHOR DECLARATIONS

### A. Conflict of interest

The authors have no conflicts to disclose.

## DATA AVAILABILITY STATEMENT

The data that support the findings of this study are available from the corresponding author upon reasonable request.

[1]J. K. Patra, G. Das, L. F. Fraceto, E. V. R. Campos, M. del Pilar Rodriguez-Torres, L. S. Acosta-Torres, L. A. Diaz-Torres, R. Grillo, M. K. Swamy, S. Sharma, S. Habtemariam, and H.-S. Shin, "Nano based drug delivery systems: Recent developments and future prospects," Journal of Nanobiotechnology **16**, 71 (2018).

[2]P. A. Netti, D. A. Berk, M. A. Swartz, A. J. Grodzinsky, and R. K. Jain, "Role of extracellular matrix assembly in interstitial transport in solid tumors." Cancer research **60**, 2497–2503 (2000).

[3]P. P. Provenzano, C. Cuevas, A. E. Chang, V. K. Goel, D. D. V. Hoff, and S. R. Hingorani, "Enzymatic targeting of the stroma ablates physical barriers to treatment of pancreatic ductal adenocarcinoma," Cancer Cell **21**, 418–429 (2012).

[4]S. Snipstad, K. Vikedal, M. Maardalen, A. Kurbatskaya, E. Sulheim, and C. de Lange Davies, "Ultrasound and microbubbles to beat barriers in tumors: Improving delivery of nanomedicine," Advanced Drug Delivery Reviews **177**, 113847 (2021).

[5]M. Afadzi, O. F. Myhre, P. T. Yemane, A. Bjørkøy, S. H. Torp, A. van Wamel, S. Lelu, B. A. J. Angelsen, and C. de Lange Davies, "Effect of acoustic radiation force on the distribution of nanoparticles in solid tumors," IEEE Transactions on Ultrasonics, Ferroelectrics, and Frequency Control **68**, 432–445 (2021).

[6]C. Einen, S. E. N. Price, K. Ulvik, M. A. Gjennestad, R. Hansen, S. Kjelstrup, and C. de Lange Davies, "Nanoparticle dynamics in composite hydrogels exposed to low-frequency focused ultrasound," Gels **9**, 771 (2023).

[7]S. Mitragotri, "Effect of therapeutic ultrasound on partition and diffusion coefficients in human stratum corneum," Journal of Controlled Release **71**, 23–29 (2001).

[8]J. Cárcel, J. Benedito, C. Rosselló, and A. Mulet, "Influence of ultrasound intensity on mass transfer in apple immersed in a sucrose solution," Journal of Food Engineering **78**, 472–479 (2007).

[9]D. Ma, J. S. Marshall, and J. Wu, "Measurement of ultrasound-enhanced diffusion coefficient of nanoparticles in an agarose hydrogel," The Journal of the Acoustical Society of America **144**, 3496–3502 (2018).

[10]H.-L. Yeh and J. J. Juárez, "Ultrasound-enhanced diffusion and streaming of colloids in porous media," Experimental Thermal and Fluid Science **121**, 110282 (2021).

[11]A. Karki, J. S. Marshall, and J. Wu, "Effect of ultrasound amplitude and frequency on nanoparticle diffusion in an agarose hydrogel," The Journal of the Acoustical Society of America **152**, 640–650 (2022).

[12]J. S. Marshall, "A model of ultrasound-enhanced diffusion in a biofilm," The Journal of the Acoustical Society of America **139**, EL228–EL233 (2016).

[13]V. Balakrishnan and G. Venkataraman, "Two-state random walk model of diffusion. 2. oscillatory diffusion," Pramana **16**, 437–455 (1981).

[14]J. Yang, J. Zhang, and J. Qiao, "Molecular dynamics simulations of atomic diffusion during the alcu ultrasonic welding process," Materials **12**, 2306 (2019).

[15]S. Zhang, Q. Li, Q. Xie, H. Zhu, W. Xu, and Z. Liu, "Mechanism analysis of heavy oil viscosity reduction by ultrasound and viscosity reducers based on molecular dynamics simulation," ACS Omega **7**, 36137–36149 (2022).

[16]M. Yu, J. Wang, Y. Yang, C. Zhu, Q. Su, S. Guo, J. Sun, Y. Gan, X. Shi, and H. Gao, "Rotation-facilitated rapid transport of nanorods in mucosal tissues," Nano Letters **16**, 7176–7182 (2016).

[17]D. B. Allan, T. Caswell, N. C. Keim, C. M. van der Wel, and R. W. Verweij, "soft-matter/trackpy: Trackpy v0.5.0," Zenodo (2021), https://doi.org/10.5281/zenodo.4682814.

[18]J. Sambrook, *Molecular Cloning: A Laboratory Manual, Third Edition, v. 1*, Vol. 1 (Cold Spring Harbor Laboratory Press, 2001).

[19]A. P. Thompson, H. M. Aktulga, R. Berger, D. S. Bolintineanu, W. M. Brown, P. S. Crozier, P. J. in 't Veld, A. Kohlmeyer, S. G. Moore, T. D. Nguyen, R. Shan, M. J. Stevens, J. Tranchida, C. Trott, and S. J. Plimpton, "LAMMPS - a flexible simulation tool for particle-based materials modeling at the atomic, meso, and continuum scales," Comp. Phys. Comm. **271**, 108171 (2022).

[20]A. Stukowski, "Visualization and analysis of atomistic simulation data with OVITO-the Open Visualization Tool," Modelling and simulation in materials science and engineering **18** (2010), 10.1088/0965-0393/18/1/015012.

[21]T. F. Willems, C. H. Rycroft, M. Kazi, J. C. Meza, and M. Haranczyk, "Algorithms and tools for high-throughput geometry-based analysis of crystalline porous materials," Microporous and Mesoporous Materials **149**, 134–141 (2012).

[22]M. Pinheiro, R. L. Martin, C. H. Rycroft, A. Jones, E. Iglesia, and M. Haranczyk, "Characterization and comparison of pore landscapes in crystalline porous materials," Journal of Molecular Graphics and Modelling **44**, 208–219 (2013).

[23]D. Frenkel and B. Smit, *Understanding Molecular Simulation: From Algorithms to Applications*, 3rd ed. (Academic Press, 2023).

[24]I. Jayawardena, P. Turunen, B. C. Garms, A. Rowan, S. Corrie, and L. Grøndahl, "Evaluation of techniques used for visualisation of hydrogel morphology and determination of pore size distributions," Materials Advances **4**, 669–682 (2023).

[25]H. Okumura and S. G. Itoh, "Amyloid fibril disruption by ultrasonic cavitation: Nonequilibrium molecular dynamics simulations," Journal of the American Chemical Society **136**, 10549–10552 (2014).

[26]V. H. Man, M. S. Li, J. Wang, P. Derreumaux, and P. H. Nguyen, "Interaction mechanism between the focused ultrasound and lipid membrane at the molecular level," The Journal of Chemical Physics **150**, 215101 (2019).

[27]V. H. Man, M. S. Li, P. Derreumaux, J. Wang, T. T. Nguyen, S. Nangia, and P. H. Nguyen, "Molecular mechanism of ultrasound interaction with a blood brain barrier model," The Journal of Chemical Physics **153**, 045104 (2020).

[28]V. H. Man, M. S. Li, P. Derreumaux, J. Wang, and P. H. Nguyen, "Molecular mechanism of ultrasound-induced structural defects in liposomes: A nonequilibrium molecular dynamics simulation study," Langmuir **37**, 7945–7954 (2021).

[29]F. E. Hajj, P. F. J. Fuchs, W. Urbach, M. Nassereddine, S. Hamieh, and N. Taulier, "Molecular study of ultrasound-triggered release of fluorescein from liposomes," Langmuir **37**, 3868–3881 (2021).

[30]M. Araki, S. Matsumoto, G.-J. Bekker, Y. Isaka, Y. Sagae, N. Kamiya, and Y. Okuno, "Exploring ligand binding pathways on proteins using hypersound-accelerated molecular dynamics," Nature Communications **12**, 2793 (2021).

[31]P. Pape and M. Praprotnik, "Dissipative particle dynamics simulation of ultrasound propagation through liquid water," Journal of Chemical Theory and Computation **18**, 1227–1240 (2022).

[32]J. Liang, M. Y. B. Zulkifli, J. Yong, Z. Du, Z. Ao, A. Rawal, J. A. Scott, J. R. Harmer, J. Wang, and K. Liang, "Locking the ultrasound-induced active conformation of metalloenzymes in metalorganic frameworks," Journal of the American Chemical Society **144**, 17865–17875 (2022).

[33]Y. Han, N. Wang, X. Guo, T. Jiao, and H. Ding, "Influence of ultrasound on the adsorption of single-walled carbon nanotubes to phenol: A study by molecular dynamics simulation and experiment," Chemical Engineering Journal **427**, 131819 (2022).

[34]W. L. Nyborg, "Acoustic streaming due to attenuated plane waves," The Journal of the Acoustical Society of America **25**, 68–75 (1953).

[35]S. H. Jamali, L. Wolff, T. M. Becker, M. de Groen, M. Ramdin, R. Hartkamp, A. Bardow, T. J. H. Vlugt, and O. A. Moultos, "OCTP: A Tool for On-the-Fly Calculation of Transport Properties of Fluids with the Order-*n* Algorithm in LAMMPS," Journal of Chemical Information and Modeling **59**, 1290–1294 (2019).

[36]D. S. Martin, M. B. Forstner, and J. A. Käs, "Apparent subdiffusion inherent to single particle tracking," Biophysical Journal **83**, 2109–2117 (2002).

[37]P. C. Chatwin, "On the longitudinal dispersion of passive contaminant in oscillatory flows in tubes," Journal of Fluid Mechanics **71**, 513–527 (1975).

[38]C. V. D. Broeck, "A stochastic description of longitudinal dispersion in uniaxial flows," Physica A: Statistical Mechanics and its Applications **112**, 343–352 (1982).

[39]K. Curran and J. S. Marshall, "Stochastic model of oscillatory diffusion for colloidal particles in a fixed porous bed," Chemical Engineering Science **246**, 116993 (2021).

[40]T. G. Leighton, *The Acoustic Bubble* (Academic Press, 1997).

[41]W. Humphrey, A. Dalke, and K. Schulten, "VMD – Visual Molecular Dynamics," Journal of Molecular Graphics **14**, 33–38 (1996).